This article was downloaded by:
On: *26 January 2011*
Access details: *Access Details: Free Access*
Publisher *Taylor & Francis*
Informa Ltd Registered in England and Wales Registered Number: 1072954 Registered office: Mortimer House, 37-41 Mortimer Street, London W1T 3JH, UK

Liquid Crystals
Publication details, including instructions for authors and subscription information:
http://www.informaworld.com/smpp/title~content=t713926090

A study on the relaxation phenomena of nematic polymers after cessation of shear flow

P. K. Chan[a]; A. D. Rey[a]
[a] Department of Chemical Engineering, McGill University, Montreal, Canada

To cite this Article Chan, P. K. and Rey, A. D.(1993) 'A study on the relaxation phenomena of nematic polymers after cessation of shear flow', Liquid Crystals, 13: 6, 775 — 795
To link to this Article: DOI: 10.1080/02678299308027293
URL: http://dx.doi.org/10.1080/02678299308027293

PLEASE SCROLL DOWN FOR ARTICLE

Full terms and conditions of use: http://www.informaworld.com/terms-and-conditions-of-access.pdf

This article may be used for research, teaching and private study purposes. Any substantial or systematic reproduction, re-distribution, re-selling, loan or sub-licensing, systematic supply or distribution in any form to anyone is expressly forbidden.

The publisher does not give any warranty express or implied or make any representation that the contents will be complete or accurate or up to date. The accuracy of any instructions, formulae and drug doses should be independently verified with primary sources. The publisher shall not be liable for any loss, actions, claims, proceedings, demand or costs or damages whatsoever or howsoever caused arising directly or indirectly in connection with or arising out of the use of this material.

LIQUID CRYSTALS, 1993, VOL. 13, NO. 6, 775–795

A study on the relaxation phenomena of nematic polymers after cessation of shear flow

by P. K. CHAN and A. D. REY*
Department of Chemical Engineering, McGill University, Montreal, Quebec H3A 2A7, Canada

(Received 28 September 1992; accepted 26 January 1993)

A viscoelastic model, composed of the Ericksen and Landau-de Gennes nematic continuum theories, is used to study numerically the relaxation phenomena after cessation of simple shear flow for a model rigid rod uniaxial nematic polymer. This model predicts that under certain conditions the relaxation of stored molecular and coupling elastic free energies due to periodic fluctuations in the scalar order parameter results in a transient periodic distortion of the director field. These conditions are that: (1) the ratio of the wavelength scales of the initial periodic spatial variation in the scalar order parameter k_S to the initial periodic planar director orientation fluctuation k_ϕ (i.e. k_S/k_ϕ) and the amplitude of the initial S spatial variation exceed certain minimum values, and (2) k_ϕ is not zero. It is shown that the wavelength selection mechanism is controlled by the director reorientation-induced backflows. The digitized optical patterns of the transient periodic director field show transient periodic optical patterns similar to the transient banded texture nematic polymers exhibit after cessation of shear flow when observed between crossed polars. The numerical results and digitized optical patterns replicate frequently reported experimental observations.

Downloaded At: 11:46 26 January 2011

1. Introduction

Strong shear flow deformations are invariably a part of nematic polymer processing, such as in the injection moulding of three dimensional objects. During processing the molecules are highly oriented along the flow direction; it is this shear flow-induced molecular orientation that gives nematic polymers their excellent mechanical properties. However, once the flow has stopped and heat treatment (i.e. solidification) has begun, the shear flow-induced molecular orientation decays away slowly [1]. During the relaxation period, the spatial distribution of the average molecular orientation, defined by a unit vector called the director **n**, may reorient into a periodic pattern along the prior shear flow direction after some finite time [2–8]. Therefore, it is of practical importance to understand the relaxation phenomena and pattern formation of nematic polymers after cessation of shear flow.

The periodic pattern mentioned above is due to a serpentine sinusoidal director field [9, 10], and only forms when the previously applied shear rate $\dot{\gamma}$ and strain γ (or shearing time t_S) exceeded certain critical values [2–8]. Depending on the material and prior shearing conditions, the pattern has a wavelength in the range of 2×10^{-6} m to 6×10^{-5} m [2, 4, 5, 10–15] and the maximum planar angle ϕ_m in the sample plane that extends from the prior flow direction to the director ranges from 8° to 45° [2, 5, 9–11, 15]. When this periodic director field is observed between crossed polars with one of the polars parallel to the flow direction, a banded texture

*Author for correspondence.

0267–8292/93 $10·00 © 1993 Taylor & Francis Ltd.

is observed [1–24]. The banded texture consists of fine, long, parallel and equidistant black lines [2], and is a characteristic property of all nematic and cholesteric polymers [6]. Recently, several investigators [3, 6, 8, 14] reported the idea of stored elastic free energy as the internal driving force for transient and spatially periodic director reorientation. Despite being well characterized, however, no definite explanation has yet been reported on the mechanism of the transient banded texture formation after cessation of shear flow for nematic polymers.

Shear flow affects the scalar order parameter S, which is a measure of the degree of molecular alignment along $\mathbf{n}$, in uniaxial nematic polymers; this can then result in spatial variations in S [25]. This idea of spatially non-homogeneous S is supported by the predicted periodic temporal oscillations of S in monodomain and spatially invariant nematic polymer systems during shear flow [25–27]. Nematic polymers also contain high concentrations of defects, which are points and lines (or disclinations) where $\mathbf{n}$ changes discontinuously [28], and this also contributes to spatial variations in S. It is then necessary to use a continuum theory that accounts for spatial variations in S when modelling numerically flows of nematic polymers.

Recently, Ericksen [29] proposed a modified version of the Leslie–Ericksen continuum theory [30–32] to accommodate static and moving defects, and to model the more complex behaviour of nematic polymers [25, 29, 33]. Examples of these complex behaviours include: (1) the formation of periodic textures during shear flow, (2) the formation of periodic textures after cessation of shear flow, (3) the first and second normal stress differences change sign from positive to negative and back to positive as the shear rate increases, (4) the viscosity increases with temperature, (5) the liquid crystal polymer (LCP) undergoes shear thickening as the shear rate is increased, and (6) the Cox–Merz rule is not obeyed. The most significant modification of the Leslie–Ericksen theory is the addition of S, and its spatial and temporal gradients. This theory has already been used lately by Calderer [34–37] to describe some salient features of nematic polymer flows. In addition, the Ericksen theory contains the essential S spiatal variation terms in the elementary static models used successfully by Barbero and Durand [38, 39] to study surface melting, by Goossens [40] to study the anchoring energy, by Galerne [41] to study the uniaxial to biaxial phase transition, and by Maddocks [42] to study static disclinations in nematic phases.

The objective of this paper is to present a numerical study of isothermal relaxation phenomena and pattern formation after cessation of steady rectilinear simple shear flow for a model incompressible uniaxial nematic polymer phase composed of rigid rod-like molecules using the Ericksen [29] and Landau–de Gennes [43] nematic continuum theories. Furthermore, this paper examines specifically the effects that an initial periodic spatial variation in S (i.e. base value S_o and amplitude A_S) have on the time for pattern formation t_b and the maximum planar orientation ϕ_m in the resulting transient periodic director configuration. Lastly, the results are discussed within the context of Frank and molecular elasticities. Partial results obtained using the model developed in the present paper are given by Chan and Rey [44].

2. Theory and balance equations

In cartesian tensorial notation for an incompressible fluid, the linear momentum balance equation is

Downloaded At: 11:46 26 January 2011

$$\rho\dot{\mathbf{V}} = \mathbf{F} + \nabla\cdot\boldsymbol{\tau}, \tag{1}$$

where ρ is the density, $\mathbf{V}$ is the velocity, and $\mathbf{F}$ is the external body force per unit volume. The superposed dot denotes the material time derivative. The constitutive equation for the stress tensor $\boldsymbol{\tau}$, according to the Ericksen theory [29], is given as

$$\begin{aligned}\boldsymbol{\tau} = &-p\boldsymbol{\delta} - \frac{\partial F_L}{\partial \nabla\mathbf{n}}\cdot(\nabla\mathbf{n})^T - \frac{\partial F_L}{\partial \nabla S}\nabla S + \beta_1(S)\dot{S}\mathbf{nn} + \alpha_1(S)(\mathbf{nn}:\mathbf{A})\mathbf{nn}\\ &+\alpha_2(S)\mathbf{nN} + \alpha_3(S)\mathbf{Nn} + \alpha_4(S)\mathbf{A} + \alpha_5(S)\mathbf{nn}\cdot\mathbf{A} + \alpha_6(S)\mathbf{A}\cdot\mathbf{nn}\end{aligned} \tag{2}$$

where the kinematic quantities are defined as follows:

$$\mathbf{A} = \frac{1}{2}[(\nabla\mathbf{V})^T + \nabla\mathbf{V}] \tag{3a}$$

$$\mathbf{N} = \dot{\mathbf{n}} - \Omega\cdot\mathbf{n} \tag{3b}$$

$$\Omega = \frac{1}{2}[(\nabla\mathbf{V})^T - \nabla\mathbf{V}]. \tag{3c}$$

The $\{\alpha_i\}$, $i=1, \ldots, 6$, and β_1 are viscosity coefficients that depend on S, p is the pressure, and $\boldsymbol{\delta}$ is the unit tensor. In addition, $\mathbf{A}$ is the rate of deformation tensor, $\mathbf{N}$ is the angular velocity of the director relative to that of the fluid, and Ω is the vorticity tensor. The ijth cartesian component of $\nabla\mathbf{n}$ and $\nabla\mathbf{V}$ are $\partial n_j/\partial x_i$ and $\partial V_j/\partial x_i$, respectively. F_L is the Landau-de Gennes free energy density expressed as follows:

$$\begin{aligned}F_L = &f_0(T) + \frac{3}{4}A(T - T_C^*)S^2 + \frac{1}{4}BS^3 + \frac{9}{16}CS^4 + \frac{3}{4}(L_1 + \frac{1}{6}L_2)(\nabla S)^2 + \frac{3}{8}L_2(\mathbf{n}\cdot\nabla S)^2\\ &+\frac{9}{4}S^2[(L_1 + \frac{1}{2}L_2)(\nabla\cdot\mathbf{n})^2 + L_1(\mathbf{n}\cdot\nabla\times\mathbf{n})^2 + (L_1 + \frac{1}{2}L_2)(\mathbf{n}\times\nabla\times\mathbf{n})^2]\\ &+\frac{3}{2}L_2S(\nabla\cdot\mathbf{n})\times(\mathbf{n}\cdot\nabla S) + \frac{3}{4}L_2S(\mathbf{n}\times\nabla\times\mathbf{n})\cdot\nabla S,\end{aligned} \tag{4}$$

where $f_0(T)$ is the isotropic free energy density at temperature T, and A, B, C, L_1 and L_2 are constants. T_C^* is a temperature slightly below the clearing temperature T_C, where the first order transition occurs. Equation (4) contains four types of terms. The first four terms contain only S, while the next two contain spatial variations of this parameter. The following term accounts for $\mathbf{n}$ spatial variations, and is expressed as such to resemble the Frank-Oseen-Zocher free energy density [43]. It should be remarked that, to second order in the Landau-de Gennes theory, there are only two independent elastic constants (L_1 and L_2); however, there are three for nematic phases [43]. The last two terms account for the couplings in the variations of S and $\mathbf{n}$. In this paper, these four terms are conveniently called the molecular free energy, the molecular elastic free energy, the Frank elastic free energy, and the coupling elastic free energy, respectively. The coefficients A, B, and C are not known for a nematic polymer. It is then convenient to replace the terms introduced by these coefficients in the free energy density by the following Maier-Saupe expression [45]

$$F_S = k_B\vartheta T\left[\frac{1}{2}\left(1 - \frac{1}{3}U\right)S^2 - \frac{1}{9}US^3 + \frac{1}{6}US^4\right], \tag{5}$$

Downloaded At: 11:46 26 January 2011

where k_B is the Boltzmann constant, ϑ is the rod concentration, and U is the dimensionless nematic potential. Now, U is the only parameter, but typical values are known [46].

The balance equations for $\mathbf{n}$ and S are defined, respectively, as follows:

$$\dot{\mathbf{n}} = \Omega \cdot \mathbf{n} + \frac{\gamma_2(S)}{\gamma_1(S)} [\mathbf{n}(\mathbf{n}^T \cdot \mathbf{A} \cdot \mathbf{n}) - \mathbf{A} \cdot \mathbf{n}] - \frac{1}{\gamma_1(S)} \frac{\delta F_L}{\delta \mathbf{n}}, \tag{6a}$$

$$\dot{S} = -\frac{1}{\beta_2(S)} \frac{\delta F_L}{\delta S} - \frac{\beta_1(S)}{\beta_2(S)} \mathbf{n}^T \cdot \mathbf{A} \cdot \mathbf{n}, \tag{6b}$$

where γ_1, γ_2 and β_2 are viscosity coefficients that depend on S. In addition,

$$\gamma_1 = \alpha_3 - \alpha_2, \tag{7a}$$

$$\gamma_2 = \alpha_6 - \alpha_5 = \alpha_2 + \alpha_3. \tag{7b}$$

The equality in equation (7*b*) is due to Parodi [47]; therefore, there are only five independent α_i viscosity coefficients. $\delta F_L/\delta(*)$ denotes the functional derivative of F_L with respect to (*). The inertia of the director is negligible and neglected.

The remainder of this section consists of the development of the partial differential equations that govern the relaxation phenomena of partially ordered nematic polymers after cessation of simple shear flow. Figure 1 shows the simple shear flow geometry, and defines the cartesian coordinate system. The upper plate velocity is V_x, ϕ is the planar director orientation angle, h is the plate spacing, and L is the sample length. It is useful to assume that the plates are infinitely wide; hence, y is the neutral direction and $\partial(*)/\partial y = 0$, where (*) denotes a dependent variable. In addition, the study in this paper is restricted to the case where the director remains parallel to the bounding plates, $\partial(*)/\partial z = 0$, $\mathbf{F} = 0$, the director reorientation-induced backflow is a creeping flow, and $V_x = V_z = 0$. Furthermore, the model presented in this paper is a viscoelastic one, where the elastic constants are dependent on S but the viscosity coefficients are not. This model then approximates the physical behaviour of uniaxial rigid rod-like nematic polymers after cessation of shear flow. More rigorous models should include the dependence of the viscosity coefficients on S, but their implementations await the availability of the required physical parameters.

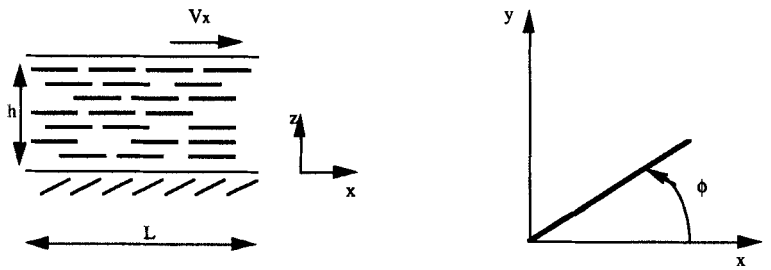

Figure 1. Schematic representation of the simple shear flow configuration, and definition of the cartesian coordinate system. The planar director orientation angle measured in radians is ϕ, V_x is the upper plate velocity, h is the plate spacing, and L is the sample length.

Downloaded At: 11:46 26 January 2011

The relaxation phenomena is best described in cartesian coordinates (see figure 1); therefore, the director field is defined as

$$\mathbf{n}=(\cos\phi,\ \sin\phi,\ 0) \tag{8}$$

where the unit length constraint, $\mathbf{n}\cdot\mathbf{n}=1$, is automatically satisfied. The velocity field during the relaxation process then simplifies to

$$\mathbf{V}=(0,\ V_y,\ 0) \tag{9}$$

and, within the planar one dimensional approximation, the three unknowns are as follows:

$$S=S(x,\ t);\qquad \phi=\phi(x,\ t);\qquad V_y=V_y(x,\ t). \tag{10\,a,\ b,\ c}$$

The three equations that govern the behaviour of V_y, ϕ and S are the y component of the linear momentum balance (see equation (1)), the z component of the angular momentum balance (see equation (6 a)), and the scalar orientational order balance (see equation (6 (b)). They are, respectively, as follows:

$$0=\eta_1\frac{\partial}{\partial x}\frac{\partial\phi}{\partial t}+\eta_2\frac{\partial\phi}{\partial x}\frac{\partial\phi}{\partial t}+\eta_3\frac{\partial\phi}{\partial x}\frac{\partial V_y}{\partial x}+\eta_4\frac{\partial}{\partial x}\frac{\partial V_y}{\partial x}, \tag{11\,a}$$

$$\eta_5\frac{\partial\phi}{\partial t}=\kappa_1\frac{\partial S}{\partial x}\frac{\partial\phi}{\partial x}+\kappa_2\frac{\partial}{\partial x}\frac{\partial\phi}{\partial x}+\kappa_3\frac{\partial}{\partial x}\frac{\partial S}{\partial x}+\eta_6\frac{\partial V_y}{\partial x}, \tag{11\,b}$$

$$\eta_7\frac{\partial S}{\partial t}=k_{\mathrm{B}}\vartheta T\left[\left(1-\frac{1}{3}U\right)S-\frac{1}{3}US^2+\frac{2}{3}US^3\right]+\kappa_4\left(\frac{\partial\phi}{\partial x}\right)^2+\kappa_5\frac{\partial}{\partial x}\frac{\partial S}{\partial x}$$
$$+\kappa_6\frac{\partial\phi}{\partial x}\frac{\partial S}{\partial x}+\kappa_7\frac{\partial}{\partial x}\frac{\partial S}{\partial x}+\kappa_8\left(\frac{\partial\phi}{\partial x}\right)^2+\kappa_9\frac{\partial}{\partial x}\frac{\partial\phi}{\partial x}+\eta_8\frac{\partial V_y}{\partial x}, \tag{11\,c}$$

where the angle-dependent viscosity functions $\{\eta_i\}$, $i=1,\ \ldots,\ 8$, and elastic functions $\{\kappa_i\}$, $i=1,\ \ldots,\ 9$, are given in the Appendix. The symbolic algebra program Theorist™ [48] was used to derive these equations.

The material physical constants used in this study are for the nematic polymer poly(4,4′-dioxy-2,2′-dimethyl azoxybenzene dodecanediyl) (DDA9) [49], and are tabulated in table 1. The sign of α_3 is not likely to alter the representative results presented below. This is due to the fact that this paper studies the relaxation phenomena after cessation of steady rectilinear shear flow; i.e. no director tumbling occurs during or after the shear flow deformation. The values for β_1, β_2, K, K_5 and K_6 are assumed, because no experimentally determined values can be found for them. The magnitudes of the three elastic constants are around the estimated value of 10^{-12} N [50]. Furthermore, the three elastic constants fulfill the constitutive hypothesis set up by Maddocks [42]

$$K_5+K_6>K. \tag{12}$$

The values for β_1 and β_2 are chosen as such so the following predicted ratios are satisfied [27, 45, 51]

$$\frac{|\beta_1|}{\gamma_1}\approx 10;\qquad \frac{\beta_2}{\gamma_1}\approx 1;\qquad \frac{|\beta_1|}{\beta_2}\cong 2 \tag{13\,a,\ b,\ c}$$

Downloaded At: 11:46 26 January 2011

Table 1. Physical constants for DDA9 [49].

Viscosities/N s m^{-2}	
α_1	-393
α_2	-415
α_3	-4
$\alpha_4+\alpha_5$	429
$\alpha_4+\alpha_6$	10
β_1†	-411×10^2
β_2†	$205{\cdot}5\times10^2$
Elastic constants/10^{-11} N	
K†$=9\,L_1+\frac{9}{2}L_2$	3·78
K_5†$=\frac{3}{2}L_1+\frac{1}{4}L_2$	3·78
K_6†$=\frac{3}{4}L_2$	37·8

†Estimated values (see text).

Downloaded At: 11:46 26 January 2011

The initial and periodic boundary conditions are as follows:

$$\phi_i=A_\phi\sin\left(k_\phi\pi x+\frac{1}{2}\pi\right)\quad\text{at } t=0,\quad 0\le x\le L, \tag{14a}$$

$$S_i=S_0+A_S\sin\left(k_S\pi x+\frac{1}{2}\pi\right)\quad\text{at } t=0,\quad 0\le x\le L, \tag{14b}$$

$$V_{y,i}=0\quad\text{at } t=0,\quad 0\le x\le L, \tag{14c}$$

$$\frac{\partial\phi}{\partial x}=0\quad\text{at } t>0,\quad x=0, \tag{14d}$$

$$\frac{\partial\phi}{\partial x}=0\quad\text{at } t>0,\quad x=L, \tag{14e}$$

$$\frac{\partial S}{\partial x}=0\quad\text{at } t>0,\quad x=0, \tag{14f}$$

$$\frac{\partial S}{\partial x}=0\quad\text{at } t>0,\quad x=L, \tag{14g}$$

$$V_y=0\quad\text{at } t>0,\quad x=0, \tag{14h}$$

$$V_y=0\quad\text{at } t>0,\quad x=L, \tag{14i}$$

where A_ϕ and A_S are the wave amplitudes, k_ϕ and k_S are the wavelength scales, and S_0 is the base value for the wave.

Equations (11 a, b, c) are solved numerically in dimensionless form. The scaling variables, dimensionless governing equations, and dimensionless initial and periodic boundary conditions are given in the Appendix. The Galerkin finite element method is used with 252 linear elements [52]. The time integrator is the first order Euler

predictor-corrector method [53], and the Newton-Raphson method is used for solving the system of non-linear algebraic equations. For all calculations, the length L is chosen as $157{\cdot}5 \times 10^{-6}$ m to accommodate sufficiently any observable periodic pattern which nematic polymers may form after cessation of simple shear flow. For a typical nematic polymer, $U = 5{\cdot}8$; the equilibrium S value is then $S_{eq} = 0{\cdot}8$ [45]. In addition, for a typical nematic polymer, the molecular length $L_m = 1{\cdot}5 \times 10^{-7}$ m and the molecular diameter $d_m = 1{\cdot}5 \times 10^{-9}$ m [54, 55]. Hence, the concentration, using the relation [45]

$$\vartheta = 1{\cdot}48 \frac{U}{L_m^2 \times d_m}$$

is $2{\cdot}53 \times 10^{23}$ rods m^{-3}. At room temperature ($T = 298$ K), the product $k_B \vartheta T = 1{\cdot}04 \times 10^3$ J m^{-3}.

3. Typical results on the relaxation phenomena

Table 2 tabulates qualitatively some of the representative results from the comprehensive study made on the relaxation phenomena of nematic polymers after cessation of shear flow [56]. By comparing the results to cases 1, 2, 6, 9, 10 and 14 with cases 3, 4, 8, 11, 12 and 16, respectively, it is noted that planar director rotation away from the prior shear flow direction only occurs if A_S exceeds a critical (or minimum) value. In addition, by comparing the results for cases 3 and 11 with cases 7 and 15, respectively, it is also noted that the ratio k_S/k_ϕ must also be greater than a minimum value. This growth is aperiodic if $k_\phi = 0$ (see cases 3, 4 and 8), but periodic if $k_\phi \neq 0$ (see cases 11, 12 and 16) initially. Since nematic polymers are known to have spatial variations in S during shear flow [25], and that transient periodic director fields are quite common phenomena in these polymers as seen in [9, 10, 57–59], the study in the remainder of this paper is based on case 16. Cases 11 and 12 are not

Downloaded At: 11:46 26 January 2011

Table 2. Some results from the study using equations (14 a, b, c) as the initial conditions ($S_0 = 0{\cdot}75$ for all cases).

Case	A_ϕ/rad	k_ϕ/m^{-1}	A_S	k_S/m^{-1}	$\lvert\phi\rvert$ Growth	Aperiodic growth	Periodic growth
1	0	$2{\cdot}1/L$	0 01	$12{\cdot}6/L$	No	N.A.	N.A.
2	0	$2{\cdot}1/L$	0·01	$126/L$	No	N.A.	N.A.
3	0	$2{\cdot}1/L$	0·108	$12{\cdot}6/L$	Yes	Yes	No
4	0	$2{\cdot}1/L$	0·108	$126/L$	Yes	Yes	No
5	0	$21/L$	0·01	$12{\cdot}6/L$	No	N.A.	N.A.
6	0	$21/L$	0·01	$126/L$	No	N.A.	N.A.
7	0	$21/L$	0·108	$12{\cdot}6/L$	No	N.A.	N.A.
8	0	$21/L$	0·108	$126/L$	Yes	Yes	No
9	0·01	$2{\cdot}1/L$	0·01	$12{\cdot}6/L$	No	N.A.	N.A.
10	0·01	$2{\cdot}1/L$	0·01	$126/L$	No	N.A.	N.A.
11	0·01	$2{\cdot}1/L$	0·108	$12{\cdot}6/L$	Yes	No	Yes
12	0·01	$2{\cdot}1/L$	0·108	$126/L$	Yes	No	Yes
13	0·01	$21/L$	0·01	$12{\cdot}6/L$	No	N.A.	N.A.
14	0·01	$21/L$	0·01	$126/L$	No	N.A.	N.A.
15	0·01	$21/L$	0·108	$12{\cdot}6/L$	No	N.A.	N.A.
16	0·01	$21/L$	0·108	$126/L$	Yes	No	Yes

included because their k_ϕs give periodic director field wavelengths that are greater than normally found in experiments for nematic polymers after cessation of shear flow [2, 4, 5, 10–13, 20].

The length scale k_ϕ gives a periodic director field wavelength of approximately $1{\cdot}5 \times 10^{-5}$ m. This is a typical wavelength, as measured experimentally, for a transient periodic director field formed after cessation of shear flow [2, 4, 5, 10–13, 20]. Furthermore, it is shown below that this wavelength is approximately the fastest growing one when compared to longer and shorter wavelengths. It turns out, as shown below that the selection mechanism depends on the director reorientation-induced backflow. The length scale k_S and amplitude A_S are chosen to represent a possible spatial variation in S. These are certainly not the only possible values; however, there are no known experimentally determined results on the spatial effects that shear flow has on S.

Figure 2 shows typical relaxation phenomena for S (first row), ϕ (second row) and the dimensionless velocity V_y^* (third row) along x^* after cessation of shear flow at $t=0{\cdot}0$ s (first column), $t=4{\cdot}0$ s (second column), $t=14{\cdot}3$ s (third column), and $t=31{\cdot}7$ s (fourth column). The initial state represents minor director fluctuations, but considerable S gradients. The relaxation of the S spatial variations after cessation of shear flow produces spatially periodic torques on the director ($t=4{\cdot}0$ s and $14{\cdot}3$ s) to reorient from the prior flow direction. Figure 3 shows the free energy per unit area as a function of time. The free energy decreases monotonically with time; hence, the transient periodic pattern is unstable. At $t=0{\cdot}0$ s, the director fluctuations and S spatial variations raise the molecular, Frank and coupling elastic free energies of the system. As time progresses, the growth and decay of a periodic director field is the fastest route for the system to release its stored molecular and coupling elastic free energies. This is primarily due to the couplings between $\mathbf{n}$ and ∇S introduced by the L_2 (or, equivalently, K_6) constant in the Landau–de Gennes free energy expression (see equation (4)). The dot product $\mathbf{n} \cdot \nabla S$ goes to zero when $\mathbf{n}$ and ∇S are orthogonal. Since ∇S is along the prior flow direction, $\nabla S \neq 0$ and only planar director orientation is considered, the magnitude of ϕ then grows. As the S spatial variations continue to decay, so do the driving torques and the director begins to reorient towards its initial state ($t=31{\cdot}7$ s). At $t \geq 31{\cdot}7$ s, $\nabla S \cong 0$; therefore, F_L reduces to the molecular free energy term (F_S) and the Frank elastic free energy term. The present fastest route that now minimizes the stored Frank elastic free energy is that where the directors reorient to a uniform orientation [56].

The response is viscoelastic since periodic director reorientation creates periodic backflow, as shown in the third row of figure 2. This is due to the initimate coupling between flow and orientation [30–32]. The phase difference of $\frac{1}{2}\pi$ rad between the ϕ and V_y^*spatial profiles is physically consistent. Maximum director rotation couples with minimum flow, and minimum director rotation couples with maximum flow. This kind of periodic coupling is seen in the magnetic reorientation of nematic polymers [57, 58]. Unlike the magnetic reorientation phenomenon, however, the sign ($\pm$) of V_y^* at $t=14{\cdot}3$ s and any position x^* switches to the opposite sign at $t=31{\cdot}7$ s; i.e. at any x^*, V_y^* becomes $(-V_y^*)$. This is due to the reversal of director rotation; at $t=14{\cdot}3$ s the directors are rotating away from x^*, but at $t=31{\cdot}7$ s the directors are rotating back to x^*. The coupling between reorientation and flow is evident in this model through:

Downloaded At: 11:46 26 January 2011

Downloaded At: 11:46 26 January 2011

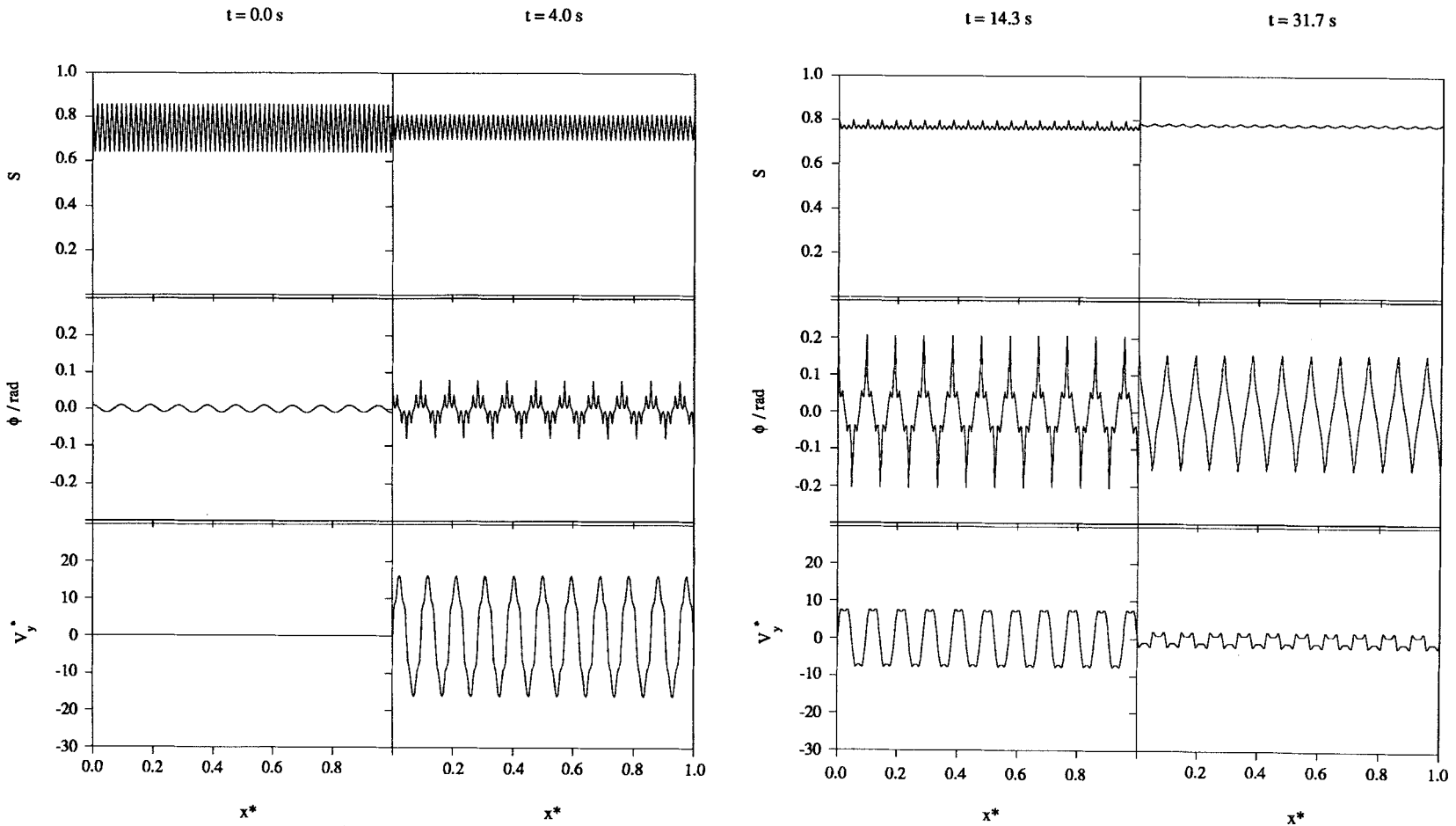

Figure 2. Scalar order parameter S (first row), planar orientation angle φ (second row) and dimensionless velocity V_y^* (third row) spatial profiles at $t = 0{\cdot}0$ s (first column), $t = 4{\cdot}0$ s (second column), $t = 14{\cdot}3$ s (third column) and $t = 31{\cdot}7$ s (fourth column).

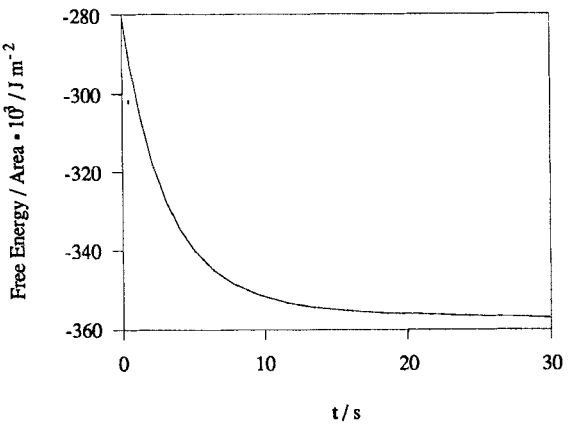

Figure 3. Transient relaxation of the stored free energy per unit area.

(1) the η_1, η_2, and η_3 terms in equation (11 *a*), and
(2) the η_6 term in equation (11 *b*).

Figure 4 shows the maximum planar orientation angle ϕ_m (first row), the maximum dimensionless velocity $V_{y,m}$* (second row) and the free energy per unit area (third row) as a function of time at the early (first column; $t \leq 30$ s) and later (second column; $t \leq 300$ s) stages of the periodic director field formation. The parameter is the director field wavelength λ_b; $\lambda_b = 5{\cdot}0 \times 10^{-6}$ m, $\lambda_b = 1{\cdot}5 \times 10^{-5}$ m and $\lambda_b = 6{\cdot}3 \times 10^{-5}$ m. From the first row of this figure, it is noticed that the periodic director field with $\lambda_b = 1{\cdot}5 \times 10^{-5}$ m is the fastest growing one when compared to longer ($\lambda_b = 6{\cdot}3 \times 10^{-5}$ m) and shorter ones ($\lambda_b = 5{\cdot}0 \times 10^{-6}$ m). There is a cross-over of the ϕ_m curves for $\lambda_b = 1{\cdot}5 \times 10^{-5}$ m and $\lambda_b = 6{\cdot}3 \times 10^{-5}$ m at $t \cong 50$ s. Since there are less elastic distortions in the latter wavelength than in the former, it will take longer for ϕ_m in the longer wavelength to relax to equilibrium. The total free energy (third row) decays similarly for the three λ_bs; therefore, for the case presented here, elasticity does not play a significant role in the wavelength selection mechanism.

Figure 5 shows the relaxation phenomena of ϕ along x* after cessation of shear flow for $\lambda_b = 5{\cdot}0 \times 10^{-6}$ m (first row), $\lambda_b = 1{\cdot}5 \times 10^{-5}$ m (second row) and $\lambda_b = 6{\cdot}3 \times 10^{-5}$ m (third row) at $t = 0{\cdot}0$ s (first column) and $t = 14{\cdot}3$ s (second column). Although the initial periodic fluctuations (first column) for the three λ_bs are quite similar, the resulting director fields at $t = 14{\cdot}3$ s are not. Further insights are obtained by studying the power spectra of the director fields. Figure 6 shows these power spectra for $\lambda_b = 5{\cdot}0 \times 10^{-6}$ m (top graph), $\lambda_b = 1{\cdot}5 \times 10^{-5}$ m (middle graph) and $\lambda_b = 6{\cdot}3 \times 10^{-5}$ m (bottom graph). They are obtained by squaring the moduli of the Fourier transforms [60] of the corresponding director fields at $t = 14{\cdot}3$ s in figure 5. The fast Fourier transform operation in MATLAB™ [61] is used for this purpose. Figure 6 shows that the director relaxation phenomenon is very different for each λ_b. There are only two modes at the shortest λ_b, four modes at the longest λ_b, but six modes at the intermediate λ_b. Periodic director rotations create periodic backflows [57, 58], which tend to increase the rate of director reorientation by reducing the magnitude of the rotational viscosity [62]. Consequently, since the intermediate wavelength has the most modes of periodic director rotation, it is then expected that this λ_b be the optimal one. Since the longest λ_b has the second largest number of

Downloaded At: 11:46 26 January 2011

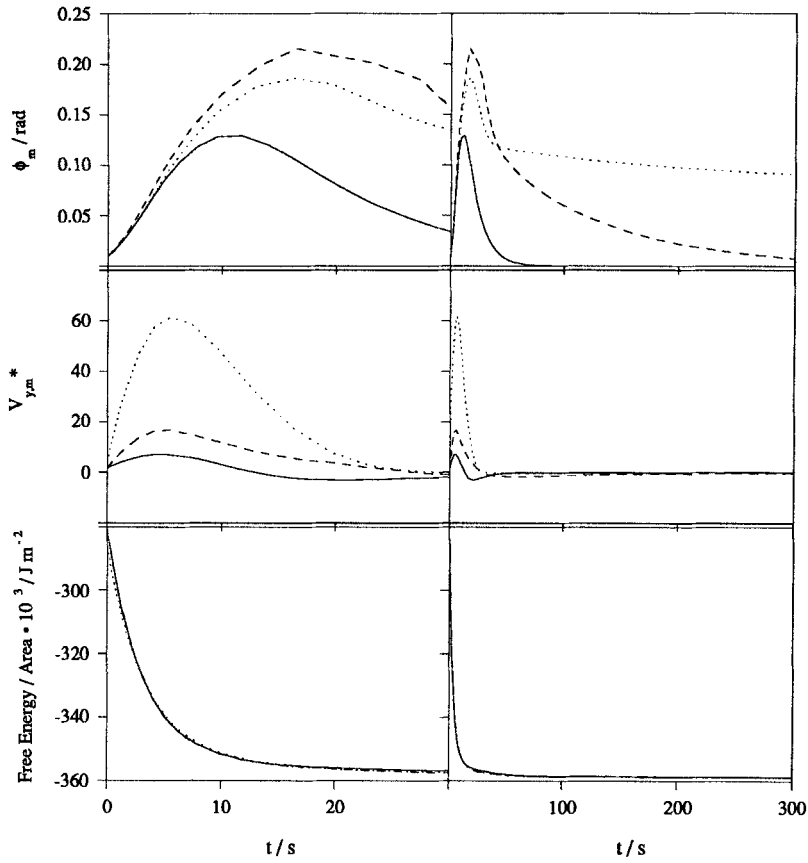

Figure 4. Maximum planar orientation angle ϕ_m (first row), maximum dimensionless velocity $V_{y,m}$* (second row) and free energy per unit area as a function of time at early (first column) and later (second column) times. The periodic director field wavelengths are: $\lambda_b = 5{\cdot}0 \times 10^{-6}$ m (———), $\lambda_b = 1{\cdot}5 \times 10^{-5}$ m (– – – –), and $\lambda_b = 6{\cdot}3 \times 10^{-5}$ m (· · · · ·).

modes, it is then expected to be the second fastest growing wavelength of the three. Lastly, since the shortest λ_b has only two modes, it is the slowest growing wavelength of the three. This is consistent with the results shown in the first row of figure 4. The results for $V_{y,m}$* shown in the second row of figure 4 is then a manifestation of the intimate coupling between the multiple modes of periodic director rotation and backflow.

4. Periodic optical patterns

Since a nematic phase has cylindrical symmetry, it is uniaxially birefringent in its natural equilibrium state; i.e. it has two refractive indices. As a result of this, a ray of light incident on the phase will be divided into two rays which vibrate orthogonally to each other and to the direction of propagation of the incident beam. They are the ordinary (O-) ray with refractive index n_0, and the extraordinary (E-) ray with refractive index n_e. Since the O- and E-rays travel at different velocities, a phase lag δ_L between the two rays is introduced as they propagate through the medium. When the sample is placed between crossed polars, an interference pattern is obtained above the analyser. The analyser allows only the vibration components of the O- and

Downloaded At: 11:46 26 January 2011

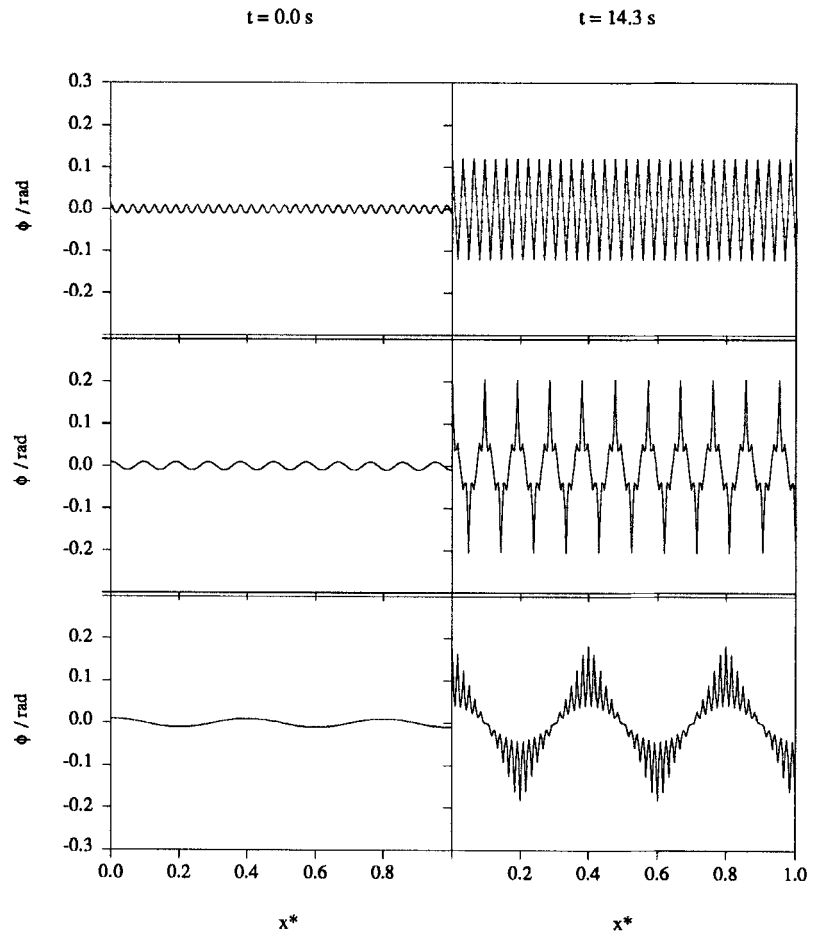

Figure 5. Spatial planar orientation angle ϕ profiles at $t=0{\cdot}0$ s (first column) and $t=14{\cdot}3$ s (second column). The periodic director field wavelengths are: $\lambda_b=5{\cdot}0\times10^{-6}$ m (first row), $\lambda_b=1{\cdot}5\times10^{-5}$ m (second row) and $\lambda_b=6{\cdot}3\times10^{-5}$ m (third row).

E-rays parallel to it to be transmitted for interference. This means that extinction (or no light transmission) only occurs when the vibration and transmission directions are orthogonal. The intensity of the interference I is [63–65]

$$I=A_L^2\sin^2(2\phi)\sin^2\left(\frac{1}{2}\delta_L\right), \tag{15}$$

where A_L is the amplitude of linearly polarized light. The phase lag is defined as

$$\delta_L=\frac{2\pi h_L(n_e-n_0)\sin^2\Phi}{\lambda_L}, \tag{16}$$

where h_L is the distance the light ray travels in the medium, λ_L is the incident light wavelength, and Φ is the angle between the incident light and the optic axis. By assuming a constant phase lag [66] in equation (15), the relative intensity I_r is

$$I_r=\sin^2(2\phi). \tag{17}$$

Downloaded At: 11:46 26 January 2011

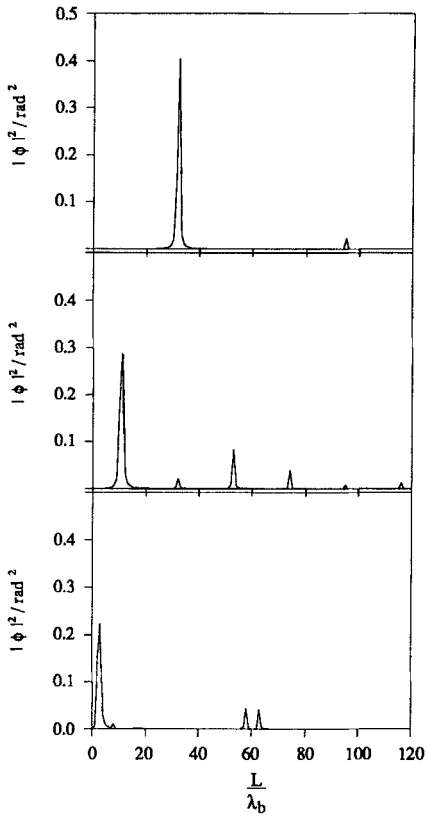

Figure 6. Power spectra of the planar orientation angle at $t=14{\cdot}3\,\text{s}$ for the following periodic director field wavelengths: $\lambda_b=5{\cdot}0\times10^{-6}\,\text{m}$ (top graph), $\lambda_b=1{\cdot}5\times10^{-5}\,\text{m}$ (middle graph) and $\lambda_b=6{\cdot}3\times10^{-5}\,\text{m}$ (bottom graph).

Figure 7 shows the digitized optical light patterns of the corresponding director fields in figure 2 obtained using equation (17). At $t=0{\cdot}0\,\text{s}$, the optical pattern is all black. This implies that the directors, as specified by the initial condition, are highly aligned along the prior shear flow direction [4]. At early times ($t=4{\cdot}0\,\text{s}$), an optical periodic pattern of weak contrast, and similar in appearance to the banded texture, begins to form. As time progresses ($t=14{\cdot}3\,\text{s}$), the directors rotate away from the prior flow direction, and the optical pattern develops into a well-defined period pattern with good contrast. It then remains for some time ($t=31{\cdot}7\,\text{s}$). The development of these optical patterns is similar to the experimental observations of the development of the banded texture formed after cessation of shear flow made by Kiss and Porter [12] and Marsano *et al.* [4]. This model, with the given physical material constants and initial and periodic boundary conditions, demonstrates that the relaxation of stored molecular elastic and coupling free energies due to periodic S spatial variations results in a transient periodic distortion of the director field, such that a transient periodic optical pattern is seen when the sample is viewed between crossed polars. Simulations employing this model can then be used to replicate several experimental observations reported in the literature on the banded texture.

Downloaded At: 11:46 26 January 2011

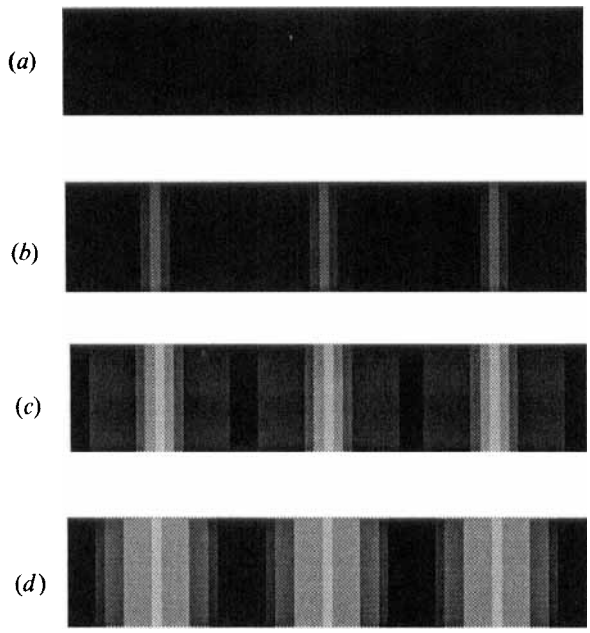

Figure 7. Time evolution of the digitized optical light patterns representing the patterns seen between crossed polars for the director fields in figure 2. The times are: (*a*) $t=0{\cdot}0$ s, (*b*) $t=4{\cdot}0$ s, (*c*) $t=14{\cdot}3$ s and (*d*) $t=31{\cdot}7$ s. The relative maximum intensity is white and the relative minimum is black.

Downloaded At: 11:46 26 January 2011

This is done by examining the effects that the base value S_0 and amplitude A_S of the initial periodic spatial variation in the scalar order parameter S have on the time for periodic director field formation t_b and the resulting maximum planar orientation angle ϕ_m for the approximate optimal wavelength determined above.

Figure 8 shows the dependence of the time for periodic director field formation t_b on the base value of the initial scalar order parameter spatial variation S_0 with the amplitude of the periodic variation A_S as the parameter; $A_S=0{\cdot}080$, $A_S=0{\cdot}095$ and $A_S=0{\cdot}108$. The time for periodic field formation decreases monotonically with increasing S_0 for a given A_S. A periodic director field is deemed subjectively [4] to be present when $I_r=0{\cdot}005$ (i.e. $\phi_m=0{\cdot}035$ rad). The region of interest for S_0 is chosen as $0{\cdot}35\leq S_0\leq 0{\cdot}75$, because $S<S_{eq}$ during shear flow [26, 27]. The region of interest for A_S is taken to be $0{\cdot}080\leq A_S\leq 0{\cdot}108$, because it represents a possible range for S spatial variations. The trends of the curves in this figure are due to the intimate coupling of director reorientation and viscous backflow. Figure 9 shows the dependence of the maximum dimensionless velocity $V_{y,m}{}^*$ on S_0 with A_S as the parameter; $A_S=0{\cdot}080$, $A_S=0{\cdot}095$ and $A_S=0{\cdot}108$. It shows that for a given A_S, $V_{y,m}{}^*$ increases monotonically with S_0. The rate of director reorientation increases with S_0 for a given A_S because $V_{y,m}{}^*$ increases; therefore, t_b decreases. Similarly, for a given S_0, the rate of director reorientation increases with A_S because $V_{y,m}{}^*$ increases; hence t_b decreases.

Figure 8 resembles very much like the frequently reported $t_b-\dot{\gamma}-t_S$ experimental plots [3–8], where t_s is the prior shearing time. It is known, from numerical predictions on monodomain and spatially invariant nematic polymer systems during

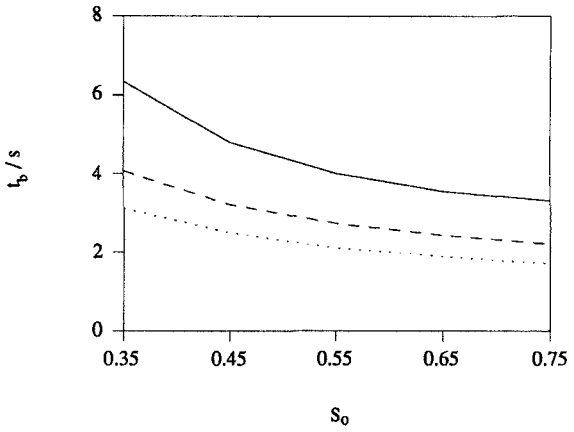

Figure 8. Time for periodic director field formation t_b as a function of the base value of the initial periodic scalar order parameter spatial variation S_0. The amplitudes of the periodic variation are: $A_S=0{\cdot}080$ (———), $A_S=0{\cdot}095$ (– – – –) and $A_S=0{\cdot}108$ (· · · ·).

Downloaded At: 11:46 26 January 2011

shear flow, that S decreases with $\dot{\gamma}$ at low shear rates but increases with $\dot{\gamma}$ at sufficiently high shear rates [26, 27]. This could then explain the fact that the banded texture only appears when $\dot{\gamma} \geq \dot{\gamma}_C$ [2–8]. In the decreasing region of the S versus $\dot{\gamma}$ relationship, the directors during shear flow are predicted to be oscillating between two orientations. Conversely, the directors are highly aligned in the flow direction in the increasing region, which is the prerequisite for banded texture formation after cessation of shear flow [3–5, 12]. Furthermore, the present model predicts that a minimum A_S is needed for periodic director field formation (see discussion for table 2). By making the plausible hypothesis that A_S increases with t_S during shear flow, the minimum A_S is then related to the critical shearing time $t_{S,C}$ needed for banded texture formation [2–8].

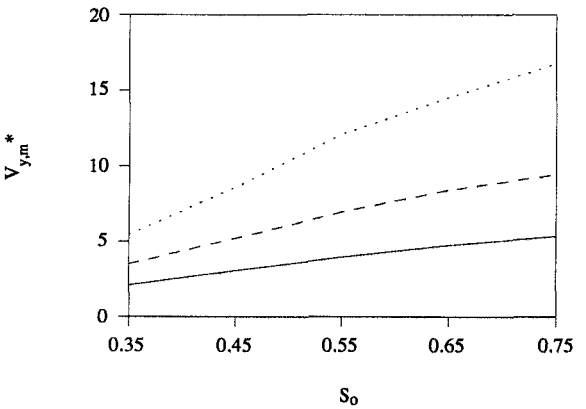

Figure 9. Maximum dimensionless velocity $V_{y,m}$* as a function of the base value of the initial periodic scalar order parameter spatial variation S_0. The amplitudes of the period variation are: $A_S=0{\cdot}080$ (———), $A_S=0{\cdot}095$ (– – – –), and $A_S=0{\cdot}108$ (· · · ·).

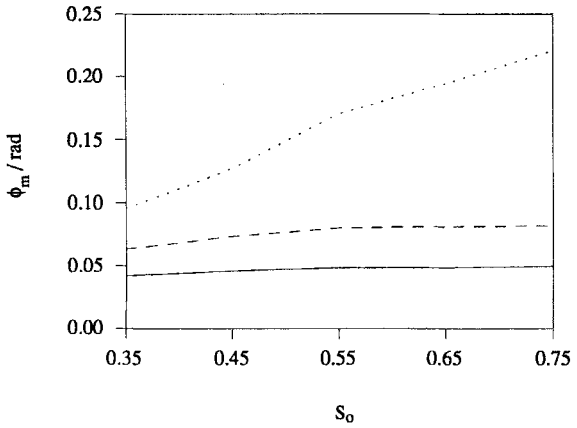

Figure 10. Maximum planar orientation angle ϕ_m as a function of the base value of the initial periodic scalar order parameter spatial variation S_0. The amplitudes of the periodic variation are: $A_S=0{\cdot}080$ (———), $A_S=0{\cdot}095$ (– – – –) and $A_S=0{\cdot}108$ (· · · ·).

Downloaded At: 11:46 26 January 2011

Figure 10 shows the dependence of the maximum planar orientation ϕ_m on the base value of the initial periodic scalar order parameter spatial variation S_0 with the amplitude of this variation A_S as the parameter; $A_S=0{\cdot}080$, $A_S=0{\cdot}095$ and $A_S=0{\cdot}108$. The maximum planar orientation increases monotonically with S_0 for a given A_S. Examples of the contrast differentials are shown in figure 11 for $A_S=0{\cdot}108$ and (*a*) $S_0=0{\cdot}35$, (*b*) $S_0=0{\cdot}55$ and (*c*) $S_0=0{\cdot}75$ at $t=14{\cdot}3$ s and in figure 12 for

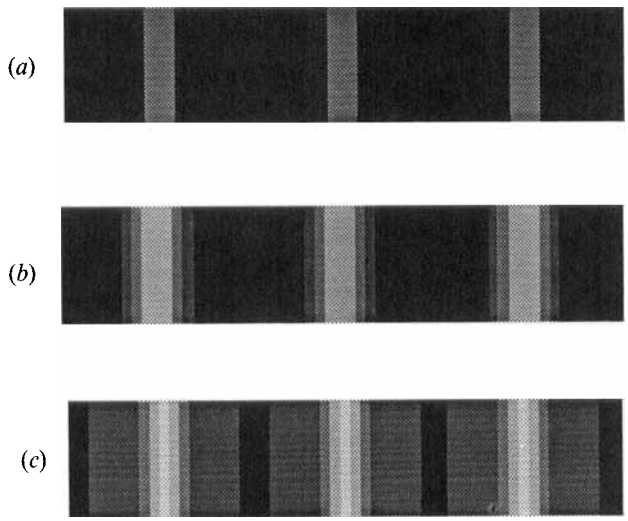

Figure 11. Digitized optical light patterns representing the patterns seen between crossed polars for the director fields at $t=14{\cdot}3$ s. The amplitude of the initial periodic scalar order parameter variation is $A_S=0{\cdot}108$, and the base values of the variation are: (*a*) $S_0=0{\cdot}35$, (*b*) $S_0=0{\cdot}55$ and (*c*) $S_0=0{\cdot}75$. The relative maximum intensity is white and the relative minimum is black.

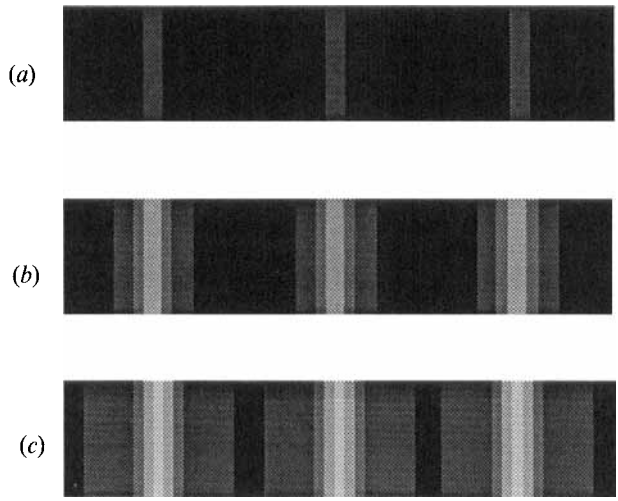

Figure 12. Digitized optical light patterns representing the patterns seen between crossed polars for the director fields at $t=14{\cdot}3$ s. The base value of the initial periodic scalar order parameter variation is $S_0=0{\cdot}75$, and the amplitudes of the variation are: (*a*) $A_S=0{\cdot}080$, (*b*) $A_S=0{\cdot}095$ and (*c*) $A_S=0{\cdot}108$. The relative maximum intensity is white and the relative minimum is black.

Downloaded At: 11:46 26 January 2011

$S_0=0{\cdot}75$ and (*a*) $A_S=0{\cdot}080$, (*b*) $A_S=0{\cdot}095$ and (*c*) $A_S=0{\cdot}108$ at $t=14{\cdot}3$ s. It is noted that the contrast of the periodic optical pattern increases with S_0 and A_S, which is consistent with the fact that S_0 is taken to scale with $\dot{\gamma}$ and the assumption that A_S scales with t_S. It is also noted that the stored molecular and coupling elastic free energies increase with either S_0 or A_S through the L_2 terms in equation (4), and that the system dissipates these energies through periodic director rotation and viscous backflow. To counter any increases in S (or, equivalently, S_0) or ∇S (or, equivalently, A_S) in these L_2 terms, $\mathbf{n}$ rotates to a greater extent away from the prior flow direction (or, equivalently, the magnitude of ϕ_m increases). Consequently, the magnitude of $\mathbf{n}\cdot\nabla S$ decreases, and by equation (17) the relative intensity (or, equivalently, contrast) increases. Once more, the intimate coupling between director reorientation and backflow is seen by observing the trends in figures 9 and 10; large (small) values of ϕ_m coincide with strong (weak) $V_{y,m}{}^*$.

5. Conclusions

The Ericksen and Landau–de Gennes continuum theories were used in this paper to study numerically the relaxation phenomena of nematic polymers after cessation of shea flow. The results presented here were restricted to show the effects that the amplitude (A_S) and base value (S_0) of the initial periodic scalar order parameter S spatial variation have on the time for periodic pattern formation (t_b) and the maximum planar director orientation (ϕ_m) in this transient pattern. Other relaxation phenomena in the presence of surface motion, disclination and surface irregularities were studied using the Leslie–Ericksen theory [30–32] and the results are available in [56]. It has been shown that the relaxation of stored molecular and coupling elastic free energies due to periodic spatial variations in S results in a transient periodic distortion of the director field, which is energetically unstable. The wavelength of

the periodic director configuration depends on the director reorientation-induced viscous backflows.

The numerical solutions, along with the digitized optical patterns, to the approximate balance equations are consistent and replicate frequently reported experimental observations of the banded texture. These observations are that the time for banded texture formation t_b decreases as the prior shear rate $\dot{\gamma}$ or prior shearing time t_s increases, and that the contrast of the banded texture increases as $\dot{\gamma}$ or t_s increases. Further work on the shear flow of nematic polymers is required to quantitatively justify the use of equation (14 *b*).

This research is supported by a grant from the Natural Sciences and Engineering Research Council of Canada (NSERC). The authors are grateful to the McGill University Computer Center for a grant to defray the computational costs of this work. P. K. Chan acknowledges his postgraduate scholarship from the NSERC.

Appendix

The viscosity functions $\{\eta_i\}$, $i=1,\ldots,4$, in equation (11 *a*) are defined as follows:

$$\eta_1=\alpha_2\cos^2\phi-\alpha_3\sin^2\phi, \tag{A 1 a}$$

$$\eta_2=-(\alpha_2+\alpha_3)\sin(2\phi), \tag{A 1 b}$$

$$\eta_3=\frac{1}{2}\alpha_1\sin(4\phi)+(\alpha_2+\alpha_3)\sin(2\phi), \tag{A 1 c}$$

$$\eta_4=\frac{1}{4}\alpha_1\sin^2(2\phi)+\frac{1}{2}(\alpha_5+\alpha_4-\alpha_2)\cos^2\phi+\frac{1}{2}(\alpha_3+\alpha_6+\alpha_4)\sin^2\phi, \tag{A 1 d}$$

The elastic functions $\{\kappa_i\}$, $i=1,\ldots,9$, and viscosity functions $\{\eta_i\}$, $i=5,\ldots,8$, in equations (11 *b*) and (11 *c*) are defined as follows:

$$\kappa_1=-KS, \tag{A 2 a}$$

$$\kappa_2=-\frac{1}{2}KS^2, \tag{A 2 b}$$

$$\kappa_3=\frac{1}{2}K_6S\sin(2\phi), \tag{A 2 c}$$

$$\kappa_4=\frac{1}{2}KS, \tag{A 2 d}$$

$$\kappa_5=-K_5, \tag{A 2 e}$$

$$\kappa_6=K_6\sin(2\phi), \tag{A 2 f}$$

$$\kappa_7=-K_6\cos^2\phi, \tag{A 2 g}$$

$$\kappa_8=K_6S\cos(2\phi), \tag{A 2 h}$$

$$\kappa_9=\frac{1}{2}K_6S\sin(2\phi), \tag{A 2 i}$$

$$\eta_5=-\gamma_1, \tag{A 2 j}$$

$$\eta_6=\frac{1}{2}[\gamma_2\cos(2\phi)-\gamma_1], \tag{A 2 k}$$

$$\eta_7=-\beta_2, \tag{A 2 l}$$

$$\eta_8=\frac{1}{2}\beta_1\sin(2\phi), \tag{A 2 m}$$

Downloaded At: 11:46 26 January 2011

where the relations

$$K=9L_1+\frac{9}{2}L_2, \tag{A 2n}$$

$$K_5=\frac{3}{2}L_1+\frac{1}{4}L_2, \tag{A 2o}$$

$$K_6=\frac{3}{4}L_2, \tag{A 2p}$$

have been used.

The dimensionless equations are obtained by scaling the elastic terms with K, the viscosity terms with γ_1, the length x with L, the velocity with $\frac{K}{\gamma_1 L}$, and the time with $\frac{\gamma_1 L^2}{K}$. By doing this, the angle-dependent viscosity and elastic functions become: $\eta_i^*=\eta_i/\gamma_1$ and $\kappa_i^*=\kappa_i/K$. The superscript asterisk denotes a dimensionless variable. Equations (11 *a*, *b*, *c*) then become the following set of dimensionless non-linear partial differential equations:

$$0=\eta_1^*\frac{\partial}{\partial x^*}\frac{\partial\phi}{\partial t^*}+\eta_2^*\frac{\partial\phi}{\partial x^*}\frac{\partial\phi}{\partial t^*}+\eta_3^*\frac{\partial\phi}{\partial x^*}\frac{\partial V_y^*}{\partial x^*}+\eta_4^*\frac{\partial}{\partial x^*}\frac{\partial V_y^*}{\partial x^*}, \tag{A 3a}$$

$$\eta_5^*=\kappa_1^*\frac{\partial S}{\partial x^*}\frac{\partial\phi}{\partial x^*}+\kappa_2^*\frac{\partial}{\partial x^*}\frac{\partial\phi}{\partial x^*}+\kappa_3^*\frac{\partial}{\partial x^*}\frac{\partial S}{\partial x^*}+\eta_6^*\frac{\partial V_y^*}{\partial x^*}, \tag{A 3b}$$

$$\begin{aligned}\eta_7^*\frac{\partial S}{\partial t^*}=&\frac{k_B\vartheta TL^2}{K}\left[\left(1-\frac{1}{3}U\right)S-\frac{1}{3}US^2+\frac{2}{3}US^3\right]+\kappa_4^*\left(\frac{\partial\phi}{\partial x^*}\right)^2\\&+\kappa_5^*\frac{\partial}{\partial x^*}\frac{\partial S}{\partial x^*}+\kappa_6^*\frac{\partial\phi}{\partial x^*}\frac{\partial S}{\partial x^*}+\kappa_7^*\frac{\partial}{\partial x^*}\frac{\partial S}{\partial x^*}+\kappa_8^*\left(\frac{\partial\phi}{\partial x^*}\right)^2\\&+\kappa_9^*\frac{\partial}{\partial x^*}\frac{\partial\phi}{\partial x^*}+\eta_8^*\frac{\partial V_y^*}{\partial x^*}.\end{aligned} \tag{A 3c}$$

Furthermore, the dimensionless initial and periodic boundary conditions are as follows:

$$\phi_i=A_\phi\sin\left(k_\phi^*\pi x^*+\frac{1}{2}\pi\right)\quad\text{at } t^*=0,\quad 0\le x^*\le 1, \tag{A 4a}$$

$$S_i=S_0+A_S\sin\left(k_S^*\pi x^*+\frac{1}{2}\pi\right)\quad\text{at } t^*=0,\quad 0\le x^*\le 1, \tag{A 4b}$$

$$V_{y,i}^*=0\quad\text{at } t^*=0,\quad 0\le x^*\le 1, \tag{A 4c}$$

$$\frac{\partial\phi}{\partial x^*}=0\quad\text{at } t^*>0,\quad x^*=0, \tag{A 4d}$$

$$\frac{\partial\phi}{\partial x^*}=0\quad\text{at } t^*>0,\quad x^*=1, \tag{A 4e}$$

$$\frac{\partial S}{\partial x^*}=0\quad\text{at } t^*>0,\quad x^*=0, \tag{A 4f}$$

$$\frac{\partial S}{\partial x^*}=0\quad\text{at } t^*>0,\quad x^*=1, \tag{A 4g}$$

Downloaded At: 11:46 26 January 2011

$$V_y^* = 0 \quad \text{at } t^* > 0, \quad x^* = 0, \tag{A 4h}$$

$$V_y^* = 0 \quad \text{at } t^* > 0, \quad x^* = 1, \tag{A 4i}$$

References

[1] WHITE, J. L., 1985, *U.S.-Japan Seminar on Polymer Liquid Crystals* (Interscience Publication), p. 241.
[2] NAVARD, P., 1986, *J. Polym. Sci. Polym. Phys. Ed.*, **24,** 435.
[3] ERNST, B., and NAVARD, P., 1989, *Macromolecules*, **22,** 1419.
[4] MARSANO, E., CARPANETO, L., and CIFERRI, A., 1988, *Molec. Crystals liq. Crystals*, **158,** 267.
[5] MARSANO, E., CARPANETO, L., CIFERRI, A., and WU, Y., 1988, *Liq. Crystals*, **3,** 1561.
[6] MARSANO, E., CARPANETO, L., and CIFERRI, A., 1989, *Molec. Crystals liq. Crystals*, **177,** 93.
[7] MARRUCCI, G., GRIZZUTI, N., and BUONAURIO, A., 1987, *Molec. Crystals liq. Crystals*, **153,** 263.
[8] MAFFETTONE, P. L., GRIZZUTI, N., and MARRUCCI, G., 1989, *Liq. Crystals*, **4,** 385.
[9] VINEY, C., DONALD, A. M., and WINDLE, A. H., 1983, *J. mater. Sci.*, **18,** 1136.
[10] NAVARD, P., and ZACHARIADES, A. E., 1987, *J. polym. Sci. polym. Phys.*, **25,** 1089.
[11] VINEY, C., DONALD, A. M., and WINDLE, A. H., 1985, *Polymer*, **26,** 870.
[12] KISS, G., and PORTER, R. S., 1980, *Molec. Crystals liq. Crystals*, **60,** 267.
[13] PEUVREL, E., and NAVARD, P., 1991, *Macromolecules*, **24,** 5683.
[14] FINCHER, C. R., 1988, *Molec. Crystals liq. Crystals*, **155,** 559.
[15] HORIO, M., ISHIWAKA, S., and ODA, K., 1985, *U.S.-Japan Seminar on Polymer Liquid Crystals* (Interscience Publication), p. 269.
[16] DONALD, A. M., VINEY, C., and WINDLE, A. H., 1983, *Polymer*, **24,** 155.
[17] DONALD, A. M., and WINDLE, A. H., 1985, *J. Mater. Sci. Lett.*, **4,** 58.
[18] KISS, G., and PORTER, R. S., 1980, *J. polym. Sci. polym. Phys. Ed.*, **18,** 361.
[19] LAUS, M., ANGELONI, A. S., FERRUTI, P., GALLI, G., and CHIELLINI, E., 1984, *J. polym. Sci. polym. Lett.*, **22,** 587.
[20] CHEN, S., JIN, Y., QIAN, R., and CAI, L., 1987, *Makromolec. Chem.*, **188,** 2713.
[21] KYOTANI, M., and KANETSUNA, H., 1982, *J. Macromolec. Sci. Phys.* B, **26** (3), 325.
[22] NISHIO, Y., YAMANE, T., and TAKAHASHI, T., 1985, *J. polym. Sci. polym. Phys.*, **23,** 1943.
[23] NISHIO, Y., YAMANE, T., and TAKAHASHI, T., 1985, *J. polym. Sci. polym. Phys.*, **23,** 1953.
[24] ZACHARIADES, A. E., NAVARD, P., and LOGAN, J. P., 1984, *Molec. Crystals liq. Crystals*, **110,** 93.
[25] MARRUCCI, G., 1991, *Liquid Crystallinity in Polymers: Principles and Fundamental Properties*, edited by A. Ciferri (VCH), Chap. 11.
[26] LARSON, R. G., 1990, *Macromolecules*, **23,** 3983.
[27] FARHOUDI, Y., 1992, Master Thesis, Department of Chemical Engineering, McGill University.
[28] DE GENNES, P. G., 1974, *The Physics of Liquid Crystals* (Clarendon Press), Chap. 4.
[29] ERICKSEN, J. L., 1989, IMA Preprint Series No. 559.
[30] ERICKSEN, J. L., 1960, *Archs Ration mech. Anal*, **4,** 231.
[31] ERICKSEN, J. L., 1961, *Trans. Soc. Rheol.*, **5,** 23.
[32] LESLIE, F. M., 1979, *Adv. Liq. Crystals*, **4,** 1.
[33] LARSON, R. G., 1988, *Constitutive Equations for Polymer Melts and Solutions* (Butterworths), Chap. 10.
[34] CALDERER, M. C., 1990, *Appl. Anal.*, **38** (4).
[35] CALDERER, M. C., 1991, *J. Rheol.* **35,** 29.
[36] CALDERER, M. C., 1990, *Proceedings of the Workshop on Defects, Singularities and Patterns in Nematic Liquid Crystals*, edited by J. M. Coron, J. M. Ghidaglia, and F. Helein, p. 25.
[37] CALDERER, M. C., 1991, *J. Non-Newt. Fluid Mech.*, **43,** 351.
[38] BARBERO, G., and DURAND, G., 1991, *Molec. Crystals liq. Crystals*, **203,** 33.
[39] BARBERO, G., and DURAND, G., 1991, *J. Phys.* II, **1,** 651.
[40] GOOSSENS, W. J. A., 1985, *Molec. Crystals liq. Crystals*, **124,** 305.
[41] GALERNE, Y., 1986, *J. Phys., Paris*, **47,** 2105.

Downloaded At: 11:46 26 January 2011

[42] MADDOCKS, J. H., 1987, *Theory and Applications of Liquid Crystals*, edited by J. L. Ericksen and D. Kinderlehrer (Springer-Verlag), p. 255.
[43] SHENG, P., and PRIESTLEY, E. B., 1974, *Introduction to Liquid Crystals*, edited by E. B. Priestley, P. J. Wojtowicz and P. Sheng (Plenum Press), Chap. 10.
[44] CHAN, P. K., and REY, A. D., 1992, *Liq. Crystals*, **12,** 1025.
[45] DOI, M., and EDWARDS, S. F., 1986, *The Theory of Polymer Dynamics* (Oxford University), Chap. 10.
[46] SIRIGU, A., 1991, *Liquid Crystallinity in Polymers: Principles and Fundamental Properties*, edited by A. Ciferri (VCH), Chap. 7.
[47] PARODI, O., 1970, *J. Phys., Paris*, **31,** 581.
[48] THEORIST™, 1989, Prescience Corporation, San Francisco, Version 1.01.
[49] MARTINS, A. F., ESNAULT, P., and VOLINO, F., 1986, *Phys. Rev. Lett.*, **57,** 1745.
[50] SHENG, P., 1974, *Introduction to Liquid Crystals*, edited by E. B. Priestley, P. J. Wojtowicz and P. Sheng (Plenum Press), Chap. 8.
[51] EDWARDS, B. J., BERIS, A. N., and GRMELA, M., 1991, *Molec. Crystals liq. Crystals*, **201,** 51.
[52] FLETCHER, C. A. J., 1984, *Computational Galerkin Methods* (Springer-Verlag), Chap 2.
[53] LAPIDUS, L., and PINDER, G., 1982, *Numerical Solution of Partial Differential Equations in Science and Engineering* (John Wiley), Chap. 4.
[54] MEYER, R. B., LONGBERG, F., TARATUTA, V., FRADEN, S., LEE, S.-D., and HURD, A. J., 1985, *Faraday Discuss. chem. Soc.*, **79,** 125.
[55] CIFERRI, A., 1982, *Polymer Liquid Crystals*, edited by A. Ciferri, W. R. Krigbaum and R. B. Meyer (Academic Press), Chap. 3.
[56] CHAN, P. K., 1992, Master Thesis, Department of Chemical Engineering, McGill University, Montreal.
[57] SRAGER, G., FRADEN, S., and MEYER, R. B., 1989, *Phys. Rev.* A, **39,** 4828.
[58] REY, A. D., 1991, *Macromolecules*, **24,** 4450.
[59] LONGBERG, F., FRADEN, S., HURD, A. J., and MEYER, R. B., 1984, *Phys. Rev. Lett.*, **52,** 1903.
[60] PRESS, W. H., FLANNERY, B. P., TEUKOLSKY, S., and VETTERLING, W. T., 1985, *Numerical Recipes* (Cambridge University Press), Chap. 12.
[61] MATLAB™, 1989, The MathWorks Inc., South Natick, Massachusetts, Version 1.2a.
[62] BROCHARD, F., 1973, *Molec. Crystals liq. Crystals*, **23,** 51.
[63] BORN, M., and WOLF, E., 1980, *Principles of Optics* (Pergamon Press), Chap 14.
[64] HARTSHORNE, N. H., 1974, *The Microscopy of Liquid Crystals* (Microscopic Publications), Chap 1.
[65] SCHIEHEL, M. F., and FAHRENSCHON, K., 1971, *Appl. Phys. Lett.*, **19,** 391.
[66] NICHOLSON, T. M., 1989, *Molec. Crystals liq. Crystals*, **177,** 163.

Downloaded At: 11:46 26 January 2011